IEEE Access
Multidisciplinary | Rapid Review | Open Access Journal

Received 22 November 2022, accepted 24 December 2022, date of publication 29 December 2022,
date of current version 5 January 2023.

Digital Object Identifier 10.1109/ACCESS.2022.3233100

RESEARCH ARTICLE

Optimal Design of Bifacial Floating Photovoltaic System With Different Installation Azimuths

BYEONG GWAN BHANG[1], JIN HEE HYUN[1], SEONG-HYEON AHN[1], JIN HO CHOI[1], GYU-GWANG KIM[2], AND HYUNG-KEUN AHN[2], (Member, IEEE)

[1]Next Generation PV Module and Power System Research Center, Konkuk University, Seoul 05029, South Korea
[2]Department of Electrical Engineering, Konkuk University, Seoul 05029, South Korea

Corresponding author: Hyung-Keun Ahn (hkahn@konkuk.ac.kr)

This work was supported in part by the New and Renewable Energy Technology Program of the Korea Institute of Energy, Technology, Evaluation, and Planning, through the financial resources by the Ministry of Trade, Industry and Energy, Republic of Korea, under Grant 20183010014260.

ABSTRACT Considering the increasing interest in the realization of carbon-neutral and RE100 systems, and the expansion of the supply of renewable energy through large-scale floating photovoltaic systems (FPVs), this study designed large-scale bifacial FPVs for maximum power density. Moreover, the estimated power generation was compared and analyzed according to the installation methods of the conventional monofacial PV module facing south (Mono-S), bifacial PV module facing south (Bi-S), and bifacial PV module facing east and west (Bi-EW). Using the proposed design method, the power generation per unit area for FPVs was 17.87% to 36.08% higher than that of the conventional installation method. In addition, this method can contribute to gird stability by decreasing the peak power around noon and increasing power generation during low irradiation and can be applicable to marine photovoltaics(MPVs).

INDEX TERMS Bifacial PV module, floating photovoltaic systems (FPVs), grid stability, maximum power density, power plant design.

I. INTRODUCTION

Photovoltaic (PV) power generation has the advantage of employing an infinite and clean energy source, but it requires a larger area per unit capacity than other power plants [1], [2]. Therefore, in countries with relatively limited land areas, such as South Korea, Japan, and Vietnam, floating PV systems (FPVs) installed on idle water surfaces are on the rise [3], [4], [5]. Particularly in Korea, 2.1 GW FPVs—the largest in the world—are scheduled to be installed in Saemangeum [6]. FPVs improve the efficiency owing to the cooling effect and efficient use of land [7], [8], [9]. Until recently, the installation cost of FPVs was high because of the high cost of buoyancy units for the PV modules. However, technological advancements have reduced the unit cost, leading to an increase in the number of FPVs [6].

In addition, to address the difficulty in securing sites for PV power plants, required for maximum power generation per unit area, several technologies have been developed for improving the efficiency of solar cells; one representative example is a bifacial solar cell [10], [11], [12]. Compared with conventional solar cells, bifacial solar cells absorb light both from the front and from the rear, thereby improving power generation [13], [14]. The application of bifacial PV module has been limited because determining the nominal power for bifacial PV modules is difficult owing to the differences in the opinions of industry and academia on the impact of rear reflection [15], [16]. However, international standards for bifacial PV modules, such as IEC 60904-1-2, have been established [17], [18], and PV systems with bifacial PV modules are emerging. The bifacial PV module generates large amounts of power even in a low irradiation environment, such as immediately after sunrise, just before sunset, and under shading conditions because of its ability to absorb light from the rear [19]. Thus, it compensates for the intermittency for PV power generation.

In general, PV power plants with conventional monofacial PV modules can generate maximum power when the installed

The associate editor coordinating the review of this manuscript and approving it for publication was Bidyadhar Subudhi.

This work is licensed under a Creative Commons Attribution 4.0 License. For more information, see https://creativecommons.org/licenses/by/4.0/

PV modules are facing south [20]. However, because PV modules are vulnerable to shading, which causes loss [21], the separation distances between the PV module strings should be sufficient, which results in an increase in the required area for the PV power plant. Particularly in the areas of middle to high latitudes, the tilt angle of the PV module should be increased to improve the efficiency of the PV power plant; this further increases the required separation distances. However, because of the advantages of the bifacial PV module, if the installed PV modules are parallel and face east and west, although the power generation per unit capacity would be reduced, the installation capacity would be increased for the same area, leading to increased power generation.

This study focused on the design of bifacial FPVs for maximum power density. To develop a design method for the maximum power density of FPVs, the installable capacity for a limited area, expected power generation, and power generation per unit area were analyzed for different installation methods—a monofacial PV module facing south (Mono-S), bifacial PV module facing south (Bi-S), and bifacial PV module facing east-west in parallel (Bi-EW). The remainder of this paper is organized as follows. Section II describes the development of the model to predict the power generation of a bifacial PV module under variations in the azimuth and tilt angles. In Section III, the power characteristics of Mono-S, Bi-S, and Bi-EW PV power systems are compared with variations in the irradiation and tilt angle. In Section IV, applications for designing large-scale bifacial FPVs are analyzed with respect to the installable capacity and power generation per unit area. Section V presents the conclusions of the study and its contributions.

II. MODELLING

A. PREDICTION OF IRRADIATION CONSIDERING THE SUN's MOTION

To predict the output of PV power systems with different azimuths, the irradiation that has the greatest effect on the amount of power generation should be predicted. Because the effective irradiation absorbed by the PV module and converted to power varies with the movement of the sun, the irradiation should be predicted considering the altitude and azimuth of the sun. Because the Earth orbits around the sun, the location where the PV modules are installed should be considered because the altitude and azimuth of the sun vary depending on the installation area, even at a specific instant of time. Fig.1 represents the relation of the PV module and the sun's position. The effective tilted irradiation that is converted to power by the PV module varies with the elevation angle (α), which is the angle between the horizontal and the sun. The elevation angle that varies depending on the declination angle (δ), latitude (ϕ), and hour angle (HRA) can be calculated as follows [22].

$$\alpha = \sin^{-1}\left[sin\delta sin\phi + \cos\delta cos\phi \cos(HRA)\right] \quad (1)$$

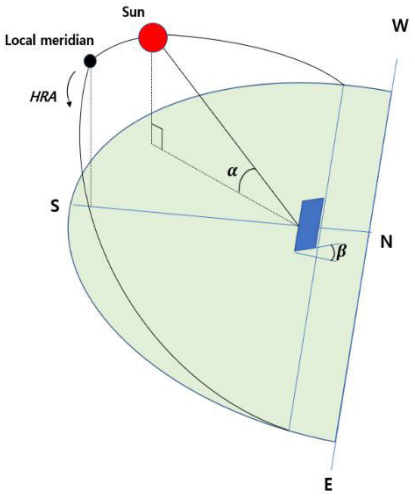

FIGURE 1. Relation of the PV module and the sun's position.

In (1), δ denotes the angle that varies seasonally owing to the rotation of the Earth around the sun and the tilt of the Earth on its axis. HRA quantifies the local solar time (LST) as the number of degrees at which the sun moves across the sky. For example, HRA at noon is defined as 0°. Because the Earth rotates 360° for a day (the same as 15° per hour), HRA is calculated as follows.

$$HRA = 15°(LST\,12) \quad (2)$$

In addition, the effective tilted irradiation varies depending on the tilt angle of the PV module and elevation angle obtained by (1). When sunlight vertically enters the plane of the PV module, power generation is maximized, but the position of the sun continues to change over time and day owing to many factors; therefore, the amount of light entering the plane varies. Fig. 2 shows the relationship between the PV module's tilt angle (β) and the amount of irradiation.

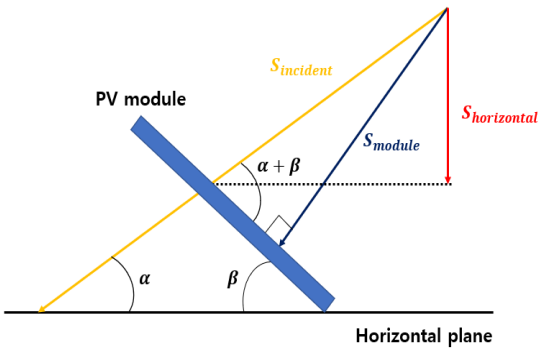

FIGURE 2. Relation of the tilted PV module and irradiation.

As shown in Fig. 2, according to the relationship between the horizontal irradiation ($s_{horizontal}$), incident irradiation ($s_{incident}$), and tilted irradiation (s_{module}), if only one type of irradiation is measured, the remaining two types of irradiation

can be calculated using (3) and (4).

$$S_{incident} = \frac{S_{horizontal}}{sin\alpha} \tag{3}$$

$$S_{module} = \frac{S_{horizontal} \times \sin(\alpha + \beta)}{\sin \alpha} \tag{4}$$

B. PREDICTION MODEL FOR BIFACIAL PVs USING VIEW FACTOR

To predict the power of the bifacial PV module, the light absorbed from both the rear and front of the PV module should be predicted. A method that uses albedo and view factors (VFs) to predict the light absorbed from the rear exists. The VF is defined as the portion of radiative heat transferred from one surface to another surface. The VF between the horizontal and inclined planes is expressed as follows [23].

$$VF = \frac{A + 1\left(A^2 + 12ACOS\alpha\right)^{\frac{1}{2}}}{2}, \tag{5}$$

where $A = h/w$

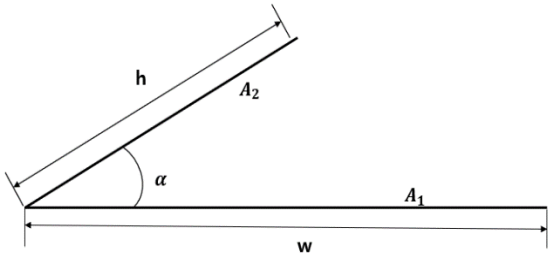

FIGURE 3. View factor between the inclined surface and the horizontal plane.

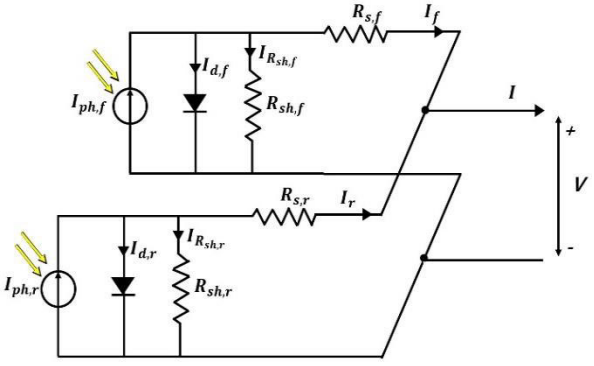

FIGURE 4. Equivalent circuit of a bifacial solar cell [19].

In Fig. 3 and (5), h can be substituted with the length of the tilted PV module plane (A_2), and w can be substituted with the length of the floor (A_1), where the PV module is installed. Fig. 4 represents the equivalent circuit of a bifacial solar cell. $I_f, I_{ph,f}, I_{d,f}, R_{sh,f}, I_{R_{sh,f}}, R_{s,f}, I_{R_{s,f}}$ in the front circuit of bifacial solar cell denote the front current, the light-generated current, the voltage-dependent current lost to recombination, the shunt resistance, the current through the shunt resistance, the series resistance, and the current through the series resistance, respectively. $I_r, I_{ph,r}, I_{d,r}, R_{sh,r}, I_{R_{sh,r}}, R_{s,r}, I_{R_{s,r}}$ in the rear circuit of bifacial solar cell denote the rear current, the light-generated current, the voltage-dependent current lost to recombination, the shunt resistance, the current through the shunt resistance, the series resistance, and the current through the series resistance, respectively.

If a bifacial PV module is represented as a double-circuit module [24], the power ($P_{bifacial}$) of the bifacial PV module can be expressed as the sum of the front power (P_{front}) and rear power (P_{rear}), as follows.

$$P_{bifacial} = P_{front} + P_{rear} \tag{6}$$

In (6), P_{front} denotes the power generated by absorbing the front light, and P_{rear} denotes the power generated by absorbing the rear light. Considering the relationship between the power, irradiation, and temperature of the PV module, (6) can be expressed as follows.

$$\begin{aligned} P_{bifacial} &= \frac{S_{module-front}}{1000} \cdot P_{STC} \cdot (1 + \delta_{P_{mpp}}(T-25)) \\ &+ \frac{S_{module-rear}}{1000} \cdot Bifi_{P_{mpp}} \cdot P_{STC} \cdot (1 + \delta_{P_{mpp}}(T-25)) \end{aligned} \tag{7}$$

In (7), $S_{module-front}$ and $S_{module-rear}$ denote the irradiation absorbed by the front and rear, respectively. P_STC denotes the power measured under Standard Test Condition(STC) (AM 1.5 G, 1000 W/m^2, 25 °C). $\delta_{P_{mpp}}$ denotes the temperature coefficient of the PV module, and T denotes the temperature of the PV module surface. $Bifi_{P_{mpp}}$ denotes the ratio of the front and rear powers of the bifacial PV module. $S_{module-front}$ is obtained by measuring directly or by calculating in (4) using the relation on the horizontal irradiation. However, if $S_{module-rear}$ is assumed to be largely composed of the sum of two lights, direct light ($S_{rear-dir.}$) and diffuse light ($S_{rear-diff.}$),it can be expressed as follows.

$$S_{module-rear} = S_{rear-dir.} + S_{rear-diff.} \tag{8}$$

In (8), $S_{rear-dir.}$ denotes the direct light reflected from the floor and entering the rear of the PV module, and $S_{rear-diff.}$ represents the scattered light in the atmosphere. $S_{rear-dir.}$ is expressed using albedo ($Alb.$) and VF of the floor. If the scattered light is assumed to be the difference between the incidental ($s_{incident}$) and the horizontal ($s_{horizontal}$) irradiation, $S_{rear-dir.}$ of these irradiations can be expressed by (9) and (10), respectively.

$$S_{rear-dir.} = S_{horizontal} \cdot Alb. \cdot VF \tag{9}$$

$$S_{rear-dir.} = -S_{incident} - S_{horizontal} \tag{10}$$

Using (7), (9), and (10), the power of the bifacial PV module can be expressed as follows.

$$\begin{aligned} P_{bifacial} &= [\frac{S_{module-front}}{1,000} \cdot P_{STC} \\ &+ \frac{S_{horizontal} \cdot Alb. \cdot VF + (S_{incident} - S_{horizontal})}{1,000} \\ &\cdot Bifi_{P_{mpp}} \cdot P_{STC}] \cdot (1 + \delta_{P_{mpp}}(T25)) \end{aligned} \tag{11}$$

C. PREDICTION MODEL FOR BI-EW CONSIDERING AZIMUTH

Generally, PV modules are installed facing south, but when installed at an arbitrary azimuth in a different direction, the irradiation is calculated considering the relationship between the azimuth of the PV module and the sun. The azimuth (θ) of the sun is expressed as follows [23].

$$\theta = \cos^{-1}\left(\frac{sin\delta cos\phi - cos\delta sin\phi \cos(HRA)}{\cos\alpha}\right) \quad (12)$$

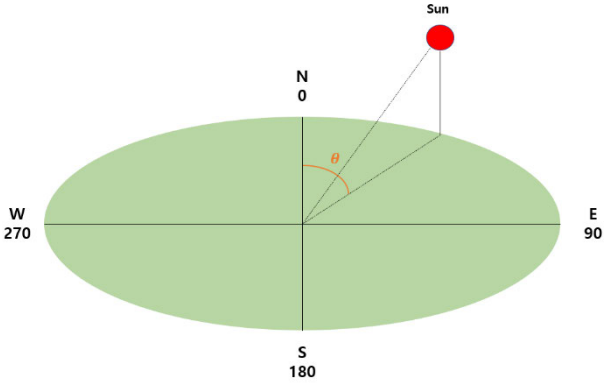

FIGURE 5. Azimuth of the sun.

Fig.5 represents the azimuth of the sun. The tilted irradiation of the PV module considering the azimuth of the sun and installation azimuth of the PV module can be expressed as follows.

$$S_{module} = S_{incident}[cos\alpha sin\beta \cos(\psi\theta) + sin\alpha cos\beta] \quad (13)$$

In (13), ψ denotes the installation azimuth of the PV module. The installation azimuth is based on 0° toward the north, 90° toward the east, 180° toward the south, and 270° toward the west. As shown in (13), when $\psi\theta = 0$, the azimuth of the sun and PV module are the same, and the irradiation can be confirmed to be maximized, leading to maximum power. The power of the bifacial PV module installed at an arbitrary azimuth can be calculated using (11) using the tilt irradiation that is calculated using (13).

III. EXPERIMENTS AND RESULT

To design FPVs that can generate maximum power in a limited area, the power characteristics of the PV power system installed in three ways—Mono-S, Bi-S, and Bi-EW—were compared and analyzed through outdoor experiments. The specifications of the PV modules used in the experiments are listed in Table 1.

For comparison, power data of Mono-S and Bi-S PV systems installed on the roof of the engineering building of Konkuk University (127.08E, 37.54N) were collected and analyzed. Fig. 6 and 7 show the 1.99 kW (248.84 W × 8 ea) Mono-S PV system and 1.77 kW (294.69 W × 6 ea) Bi-S PV system, respectively.

The powers of the Bi-E and Bi-W PV modules were measured by installing two holders, as illustrated in Fig. 8.

TABLE 1. Specifications of PV modules for experiments.

	P_{mpp} [W]	I_{sc} [A]	V_{OC} [V]	I_{mpp} [A]	V_{mpp} [V]	$F.F$ [-]	$bifi_{P_{mpp}}$ [-]
Mono-S	248.84	8.81	37.70	8.26	30.13	0.75	-
Bi-S	294.69	9.84	39.88	8.92	33.04	0.75	0.66
Bi-E	327.84	9.09	46.84	8.57	38.26	0.77	0.79
Bi-W	328.98	9.13	46.95	8.59	38.31	0.77	0.81

FIGURE 6. PV power system with 1.99 kW Mono-S.

FIGURE 7. PV power system with 1.77 kW Bi-S.

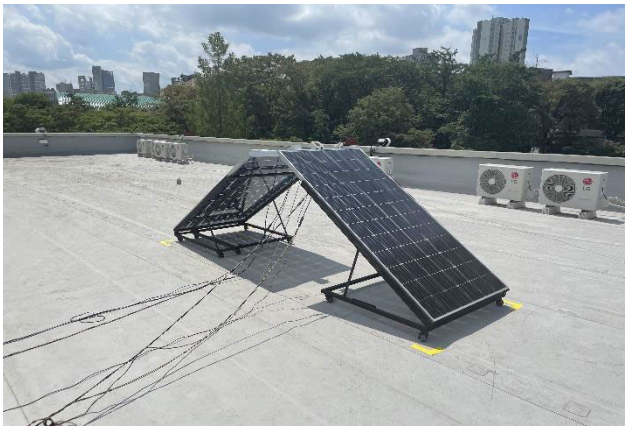

FIGURE 8. PV power system with 0.66 kW Bi-EW.

The power of the Bi-EW PV power system was assumed to be the sum of the powers of the Bi-E and Bi-W PV modules. The power of the Bi-EW cannot be considered as the simple sum of the power of the Bi-E and Bi-W PV modules because of the power mismatch when connected in series. However, when designing large-scale FPVs, which is the final goal of this study, the Bi-E and Bi-W PV modules are assumed to be

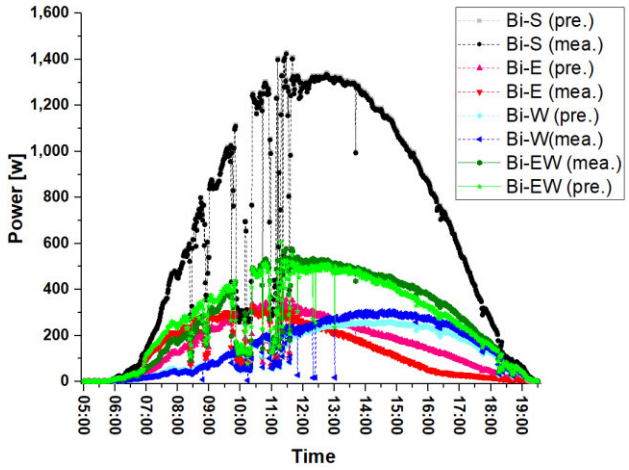

FIGURE 9. Comparison of the measured and predicted powers for the PV power system with a tilt angle of 30°.

connected to separate inverters; therefore, the power of Bi-EW is assumed to be the sum of the two modules. Fig. 9 shows the daily predicted and measured powers of Bi-S, Bi-E, Bi-W, and Bi-EW at a tilt angle of 30°, at which the maximum power generation could be produced in the test bed.

The mean absolute percentage error (MAPE) of power prediction for Bi-S was approximately 10%, and the MAPE for Bi-E and Bi-W was approximately 20%. The performance of the prediction model was assumed to be distorted because the error rate of the measured irradiation and the resulting error of the predicted power generation appeared relatively large at the time of low irradiation, such as immediately after sunrise and just before sunset. Considering this, when the root mean square error (RMSE) was calculated, the RMSE for Bi-S was 72.8 W, showing an error of approximately 4.11% considering its capacity (1,770 W). In addition, the total daily power generation, which is an integral value for power by time, had an error rate of 0.63%, showing a relatively high predictive performance. Furthermore, the RMSE of power for Bi-E and Bi-W was approximately 20 W and considering the capacity of Bi-E and Bi-W, their error rates could be estimated to be 5.21% and 6.44%, respectively. Consequently, the RMSE of power for Bi-EW was 32.23 W, an error rate of approximately 4.91% could be estimated by considering the capacity, and the error rate of daily power generation was 1.61%.

The error rate of the instantaneous power was measured to be relatively large owing to the error in the irradiation measurement. Because tilt irradiation is measured in PV power plants, the predicted power using the measured tilt irradiation of the Bi-E and Bi-W PV modules and the measured power were compared, as shown in Fig. 10.

Although the error rates in Table 2 do not appear to differ significantly from the indicators in Table 3, Figs. 9 and 10 show that the error between the measured and predicted powers using the measured tilt irradiation of the Bi-E and Bi-W PV modules is significantly reduced. Consequently,

TABLE 2. Comparison of the error rates for the prediction model of the PV power system with a tilt angle of 30°.

	Capacity [W]	MAPE [%]	RMSE [W]	Error rate of daily power generation [%]
Bi-S	1,770	10.25	72.80	-0.63
Bi-E	327.84	22.00	17.08	-13.65
Bi-W	328.98	20.80	21.17	8.83
Bi-EW	656.82	15.21	32.23	-1.61

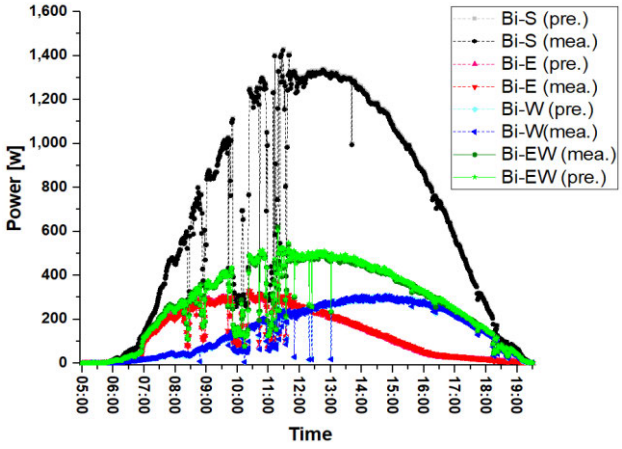

FIGURE 10. Comparison of the measured and predicted powers based on the measured irradiation for the PV power system with a tilt angle of 30°.

TABLE 3. Comparison of the error rates for the prediction model based on the measured irradiation for the PV power system with a tile angle of 30°.

	Capacity [W]	MAPE [%]	RMSE [W]	Error rate of daily power generation [%]
Bi-S	1,770	10.25	73.00	-0.63
Bi-E	327.84	22.00	17.08	1.23
Bi-W	328.98	20.80	21.17	0.11
Bi-EW	656.82	15.21	32.23	0.63

the error rate of the daily power generation for Bi-EW was approximately 0.63%. The relatively high error in the performance index was largely owing to the influence of the measured distortion value in the low-irradiation range. Fig. 11 shows the daily power of the Mono-S, Bi-S, and Bi-EW PV power systems converted to the same capacity.

As shown in Fig. 11, the difference in the generated power at noon, a relatively high irradiation time, in the power generation of the three PV power systems was not large, but the power generation was large in the order of Mono-S < Bi-S < Bi-EW in the time after sunrise and just before sunset owing to generation by the rear of the bifacial PV module.

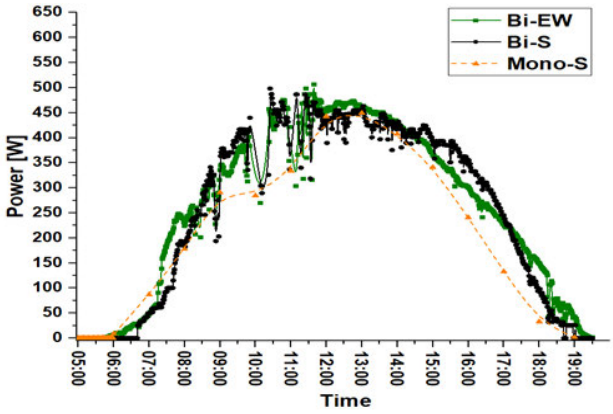

FIGURE 11. Daily power for the Mono-S, Bi-S, and Bi-EW PV power systems with a tilt angle of 30°.

This is believed to contribute to the stable operation of the power grid by supplementing intermittency, a disadvantage of solar power generation.

In another case, the predicted and measured powers of the PV power system were compared, where the PV module was installed with a tilt angle of 15°; this was installed to ensure stability from typhoons in the mid-latitude region. Fig. 12 shows the daily predicted and measured powers of Bi-S, Bi-E, Bi-W, and Bi-EW at a tilt angle of 15°.

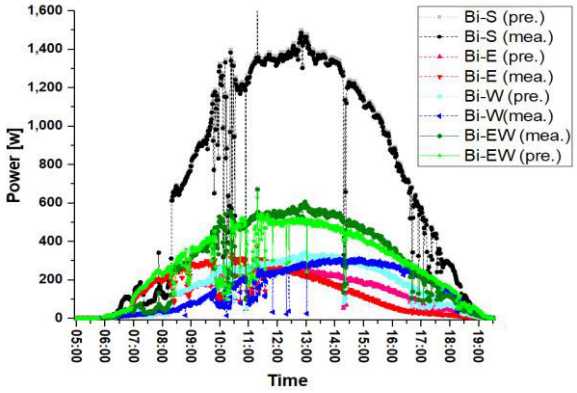

FIGURE 12. Comparison of the measured and predicted powers for the PV power system with a tilt angle of 15°.

Table 4 presents a comparison of the error rates for the prediction model of the PV power system with a tilt angle of 15°.

As in the case of a tilt angle of 30°, the measured and predicted powers using the measured tilt irradiation of the Bi-E and Bi-W PV modules were compared, as presented in Table 5 and Fig. 13.

Notably, with the use of tilt irradiation for Bi-E and Bi-W, the error rates of instantaneous power and daily power generation were relatively small. In summary, the power of Bi-S, Bi-E, Bi-W, and Bi-EW could be predicted by measuring only the horizontal irradiation. However, if the tilt irradiation of Bi-E and Bi-W could be measured,

TABLE 4. Comparison of the error rateS for the prediction model of the PV power system with a tilt angle of 15 °.

	Capacity [W]	MAPE [%]	RMSE [W]	Error rate of daily power generation [%]
Bi-S	1,770	30.86	177.20	-1.14
Bi-E	327.84	66.33	58.86	6.06
Bi-W	328.98	57.19	52.04	10.81
Bi-EW	656.82	34.12	67.33	8.60

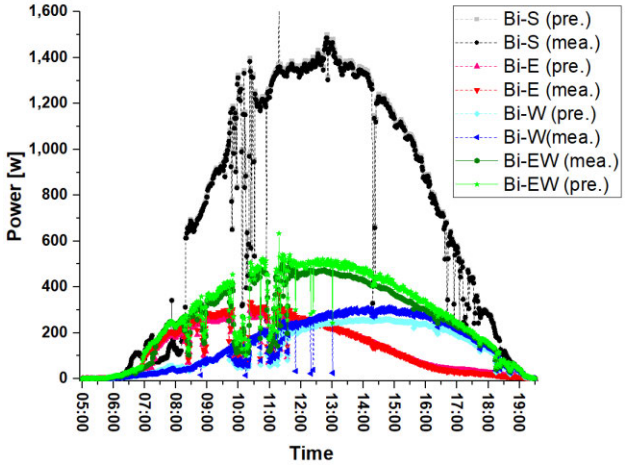

FIGURE 13. Comparison of the measured and predicted powers based on the measured irradiation for the PV power system with a tilt angle of 15°.

TABLE 5. Comparison of the error rates for the prediction model based on the measured irradiation for the PV power system with a tile angle of 15°.

	Capacity [W]	MAPE [%]	RMSE [W]	Error rate of daily power generation [%]
Bi-S	1,770	30.86	177.20	-1.14
Bi-E	327.84	17.14	13.81	2.00
Bi-W	328.98	18.29	23.56	-7.28
Bi-EW	656.82	11.08	25.70	-2.96

the power generation could be predicted with a higher accuracy. Fig. 14 shows the daily power for the Mono-S, Bi-S, and Bi-EW PV power systems converted to the same capacity.

As the tilt angle of the PV module was lowered, although the bifacial PV system generated more power than the monofacial PV system, the east-west installation of the PV module had little effect on increasing power generation. Therefore, when designing large-scale FPVs, the maximum power density should be designed by considering the change in the required area and power generation depending on the tilt angle of the PV module.

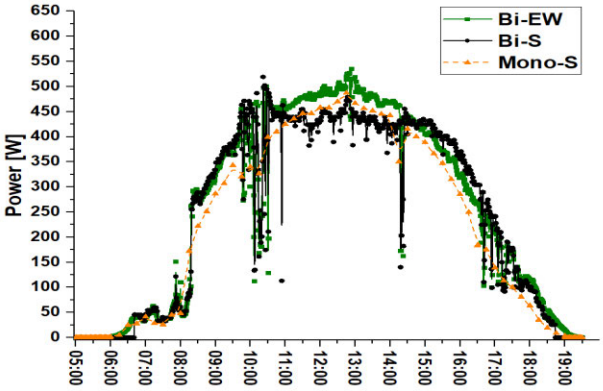

FIGURE 14. Daily power for the Mono-S, Bi-S, Bi-EW PV power systems with a tilt angle of 15°.

IV. APPLICATION

To study the feasibility of the Bi-EW installation method to maximize power generation per unit area, the installation methods of Mono-S, Bi-S, and Bi-EW were applied to compare the installable capacity and expected power generation according to the installation methods. The changes in the installable capacity of Bi-S and Bi-EW in the area required to install 100 MW by the Mono-S installation method, the conventional installation method, were compared. The specifications of the design are listed in Table 6.

TABLE 6. Specifications of the PV module for design.

	SPECIFICATION
Type of solar cell	Monocrystalline
Maximum power point power	570 W
Open circuit voltage	53.59 V
Short circuit current	13.49 A
Maximum power voltage	44.46 V
Maximum power current	12.83 A
Maximum system voltage	1,500 V
Dimension	2,416 × 1,134 × 35 mm^3
Weight	34.4 kg
Efficiency	20.8%
Bifaciality	0.7

To design 100 MW FPVs, one floating block was configurated with 2.5 MW, as presented in Table 7.

TABLE 7. Composition of 2.5 MW block in FPVs.

Components	Specifications
PV modules	4,320 ea (24 series × 180 parallel)
PV combiner	10 ea (18 ch)
PV inverter	2,500 kVA (2,500 kVA × 1 ea)
Block capacity	2,4624 MW (570 W × 24 series × 180 parallel)

The location of the large-scale FPVs was assumed to be Saemangeum (35.86°N, 126.54°E), where 2.1 GW FPVs are planned to be installed, as shown in Fig. 15.

The location and weather conditions of Saemangeum are listed in Table 8.

FIGURE 15. Location of Saemangeum for large-scale FPVs [25].

TABLE 8. Location and weather conditions of Saemangeum.

	Details
Latitude	35.89°
Longitude	126.57°
Annual horizontal irradiation	1,324.61 kWh/m²
Annual average temperature	13.0°C
Annual average humidity	77.8%
Annual average wind speed	2.2 m/s

Considering the location of Saemangeum, the PV modules were designed with a tilt angle of 30° and a shading angle of 22°. Table 9 presents a comparison of the arrangement and required area of floating units (2 × 9 [ea] PV modules) by Mono-S, Bi-S, and Bi-EW installation methods considering the tilt and shade angles of the solar module.

TABLE 9. Comparison of floating units according to the installation methods.

		Mono-S	Bi-S	Bi_EW
View	Front	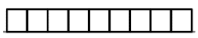		
	Plane	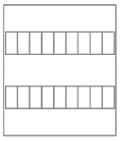		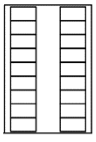
Capacity per area [kW/m^2]		0.07823		0.1342
Area required for 100 MW		1.9253		1.2664
Ratio for area requirement compared to Mono-S [%]		100	100	65.78

Fig. 16 shows a comparison of the PV module arrangement and installable capacity of Mono-S, Bi-S, and Bi-S in the same area; 100 MW (98.496 MW) installable area by Mono-S installation.

The area required to install PV modules with a capacity of 100 MW (98.496 MW) is estimated to be 1.9253 km^2 However, a PV module with a capacity of 137.8944 MW was

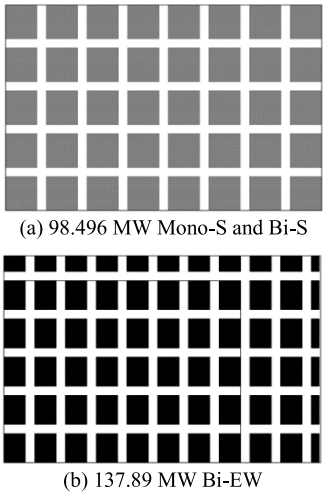

FIGURE 16. Comparison of the PV module arrangement and capacity according to the installation methods in the same area.

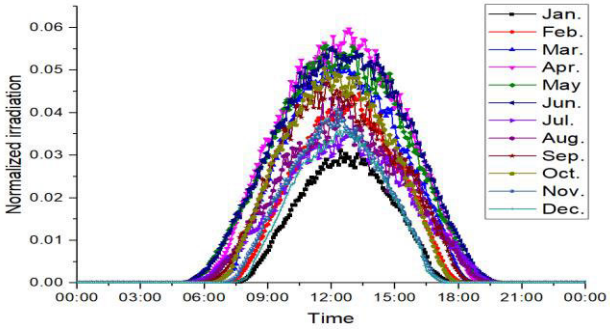

FIGURE 17. Distribution of monthly horizontal irradiation.

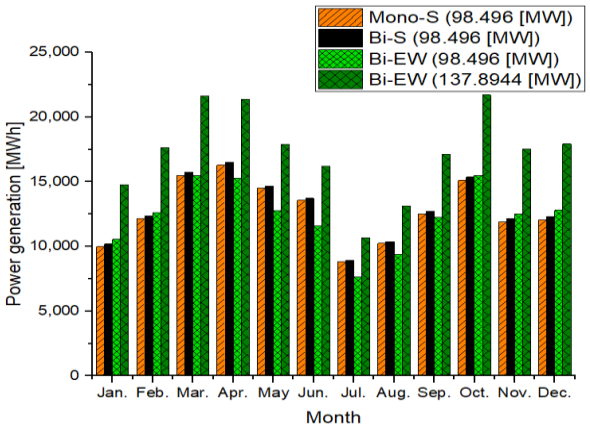

FIGURE 18. Monthly power generation according to the installation methods and capacity (tilt angle of 30°).

TABLE 10. Comparison of PV power generation for installation methods.

	Mono-S	Bi-S	Bi-EW
Capacity [MW]	98.496	98.496	137.8944
Power generation [MWh]	143,440.62	145,747.54	195,189.30
Average daily power generation time [h]	3.99	4.05	3.88
Ratio to Mono — Daily generation time	1.02	0.97	
Ratio to Mono — Power generation	1.02	1.36	
Power generation per unit area [MWh/ km^2]	79,225.25	80,499.41	107,807.10

assumed to be installed by the Bi-EW installation method. This showed the effect of increasing the installable capacity of the PV modules by approximately 40%. Power generation according to the installation methods was calculated using the installable capacity for each installation method and collected irradiation of Saemangeum. Fig. 17 shows the distribution of average horizontal irradiation over 30 years (1992–2021) in Saemangeum; this data was collected from the Korea Meteorological Administration.

Fig. 18 shows the monthly power generation according to the installation methods.

Table 10 presents a comparison of annual power generation considering the installable capacity according to the installation methods.

From the perspective of the average daily power generation time, Bi-EW appeared inefficient among the three installation methods. This is because, as shown in Fig. 18, the power of Bi-EW is the lowest in summer when the sun's altitude is high, and a significant amount of irradiation exists because the influence of front irradiation increases compared with the irradiation that can be absorbed into the rear of the PV module. However, in terms of power density, because the installable capacity of Bi-EW was the largest in the same area, the total power generation of Bi-EW was the largest. In other words, the Bi-EW installation method could maximize the power density. In addition, by installing the Bi-EW method, the peak power of the PV system was lowered, reducing the burden on the power grid. This could be confirmed by comparing the power generation according to the installation methods for the same capacity, as shown in Fig. 18. In addition, this could partially compensate for the intermittency of PV power generation by generating relatively high power even in low-irradiation environments, such as immediately after sunrise or just before sunset.

In another case, the power density was compared when the tilt angle of the PV module was lowered from 30° to 12° in the same area. Fig. 19 shows the floating PV unit for each tilt angle.

When the tilt angle of the PV module was lowered from 30° to 12°, the unit area of the Bi-S installation method significantly reduced, but the unit area of Bi-EW slightly increased because the space between Bi-E and Bi-W was separated by the same separation distance to be used as a path for maintenance. Fig. 20 shows a comparison of the PV module arrangement and installable capacity considering a unit with a tilt angle of 12°.

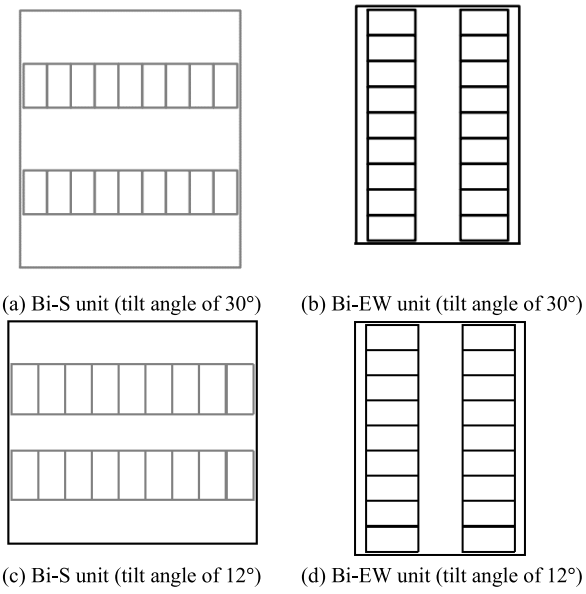

FIGURE 19. Comparison of floating PV units by tilt angle.

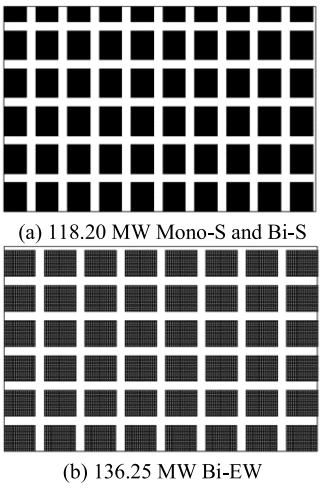

FIGURE 20. Comparison of the PV module arrangement and capacity according to the installation methods in the same area (tilt angle of 12°).

Fig. 21 shows the monthly power generation according to the installation methods, considering the installable capacity.

Table 11 presents a comparison of annual power generation considering the installable capacity according to the installation methods.

As the tilt angle of the PV module was lowered, the tilt irradiation of the front decreased, and the daily average power generation time decreased for all installation methods. In addition, as the tilt irradiation of the front decreased, the influence of rear irradiation relatively increased, and the power generation time was the largest in the Bi-EW installation method compared with that of the Mono-S and Bo-S installation methods, unlike the 30° tilt angle case. The power density of Bi-EW was greater than those of Mono-S and Bi-E, although it was smaller than that for the tilt angle of 30°.

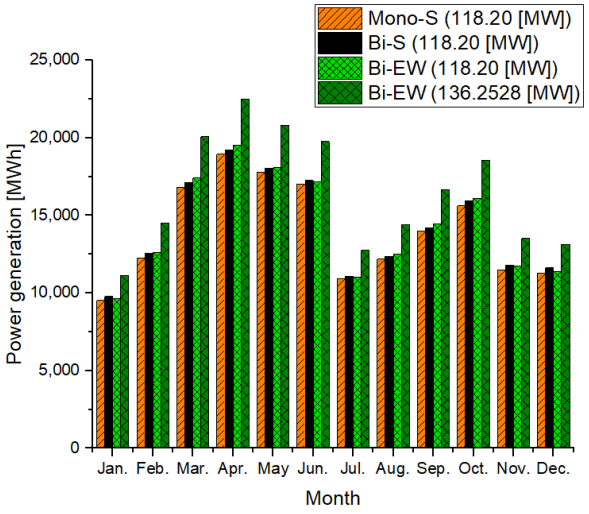

FIGURE 21. Monthly power generation according to the installation methods and capacity (tilt angle of 12°).

TABLE 11. Comparison of PV power generation for installation methods.

		Mono-S	Bi-S	Bi-EW
Capacity [MW]		118.1952	118.1952	136.2528
Power generation [MWh]		157,827.41	160,768.99	186,030.03
Average daily power generation time [h]		3.66	3.73	3.74
Ratio to Mono	Daily generation time	1.02	0.97	
	Power generation	1.18	1.36	
Power generation per unit area [MWh/ km^2]		81,975.49	83,503.35	96,623.92

V. CONCLUSION

This study compared the installable capacity and estimated power generation according to the conventional installation methods (Mono-S, Bi-S, Bi-EW) to maximize the power density of large-scale FPVs with bifacial PV modules. To calculate the expected power generation of large-scale FPVs for each installation method, power prediction was modeled through irradiation according to the tilt angle, azimuth, and rear irradiation obtained using the VF. The expected power generation showed an error rate of 0.63% to 13.65%, and the expected power generation based on the measured tile irradiation of the PV module facing east and west showed an error rate of 0.11% to 7.28%. Comparing the arrangement of PV modules considering the separation distances between PV module arrays for the installation methods, the installable capacity of Bi-EW under the required area for 100 MW FPVs with PV modules facing south was

calculated to be 15% to 40% higher depending on the tilt angle of the PV module (12° to 30°). Compared with the conventional Mono-S installation method with Bi-EW, the expected annual power generation density obtained using the installable capacity and power prediction model was calculated to be at 81,975.49 to 96,623.92 MWh/ km^2 with a tilt angle of 12° and 79,225.25 to 107,807.10 MWh/ km^2 with a tilt angle of 30°, showing that the power density was 17.87% to 36.08% higher.

Currently, in some countries, the ratio of the area for the installation of FPVs to the water surface is limited owing to concerns about water quality and habitats of migratory birds. This study on the maximum power density will contribute to expanding the power generation of renewable energy from FPVs to MPVs(Marine Photovoltaics). In addition, operating the power grid is difficult owing to the intermittency in PV power generation depending on weather conditions. This study will contribute to the stable operation of power grids by lowering the peak power around noon and increasing the power generation under low irradiation conditions. MPVs is under research and development worldwide as an expansion of FPVs. For the further study, economic analysis considering the estimated power generation and total investment cost by Bi-EW installation methods would be conducted for the feasibility and this method could be applied to the MPVs as well.

REFERENCES

[1] S. Ong, "Land-use requirements for solar power plants in the United States," Nat. Renew. Energy Lab. (NREL), Golden, CO, USA, Tech. Rep., NREL/TP-6A20-56290, 2013.

[2] M. Bolinger and G. Bolinger, "Land requirements for utility-scale PV: An empirical update on power and energy density," *IEEE J. Photovolt.*, vol. 12, no. 2, pp. 589–594, Mar. 2022, doi: 10.1109/JPHOTOV.2021.3136805.

[3] M. Abid, Z. Abid, and M. Umer, "Floating photovoltaic system technology-prospects of its implementation in central Asian, South Asian and South East Asian Region," in *Energy and Environmental Security in Developing Countries*. Cham, Switzerland: Springer, 2021, pp. 633–658.

[4] H. Pouran, M. P. C. Lopes, H. Ziar, D. A. C. Branco, and Y. Sheng, "Evaluating floating photovoltaics (FPVs) potential in providing clean energy and supporting agricultural growth in Vietnam," *Renew. Sustain. Energy Rev.*, vol. 169, Nov. 2022, Art. no. 112925.

[5] C. M. Ahn, J. C. Joo, J. H. Kim, S. H. Choi, J. S. Jang, and H. W. Go, "Review of installation status and major environmental issues of floating photovoltaic power plants (FPVs)," *J. Korean Soc. Environ. Eng.*, vol. 43, no. 4, pp. 286–298, Apr. 2021.

[6] M. Kumar, H. M. Niyaz, and R. Gupta, "Challenges and opportunities towards the development of floating photovoltaic systems," *Sol. Energy Mater. Sol. Cells*, vol. 233, Dec. 2021, Art. no. 111408.

[7] A. El Hammoumi, A. Chalh, A. Allouhi, S. Motahhir, A. El Ghzizal, and A. Derouich, "Design and construction of a test bench to investigate the potential of floating PV systems," *J. Cleaner Prod.*, vol. 278, Jan. 2021, Art. no. 123917.

[8] W. C. L. Kamuyu, J. Lim, C. Won, and H. Ahn, "Prediction model of photovoltaic module temperature for power performance of floating PVs," *Energies*, vol. 11, no. 2, p. 447, Feb. 2018.

[9] B. Bhang, G. Kim, H. Cha, D. Kim, J. Choi, S. Park, and H. Ahn, "Design methods of underwater grounding electrode array by considering inter-electrode interference for floating PVs," *Energies*, vol. 11, no. 4, p. 982, Apr. 2018.

[10] T. Sugiura, S. Matsumoto, and N. Nakano, "Bifacial PERC solar cell designs: Bulk and rear properties and illumination condition," *IEEE J. Photovolt.*, vol. 10, no. 6, pp. 1538–1544, Nov. 2020, doi: 10.1109/JPHOTOV.2020.3013987.

[11] R. Kopecek, J. Libal, J. Lossen, V. D. Mihailetchi, H. Chu, C. Peter, F. Buchholz, E. Wefringhaus, A. Halm, J. Ma, L. Jianda, G. Yonggang, Q. Xiaoyong, W. Xiang, and D. Peng, "ZEBRA technology: Low cost bifacial IBC solar cells in mass production with efficiency exceeding 23.5%," in *Proc. 47th IEEE Photovoltaic Spec. Conf. (PVSC)*, Jun. 2020, pp. 1008–1012, doi: 10.1109/PVSC45281.2020.9300503.

[12] M. J. Yun, Y. H. Sim, D. Y. Lee, and S. I. Cha, "Enhancement electricity producion in same ground area by curved tessellated bifacial Si solar cells," in *Proc. IEEE 48th Photovoltaic Spec. Conf. (PVSC)*, Jun. 2021, pp. 0573–0575, doi: 10.1109/PVSC43889.2021.9518822.

[13] S. M. Kim, "A study of performance characterization with rear light source in conventional bifacial solar cells," in *Proc. IEEE 44th Photovoltaic Spec. Conf. (PVSC)*, Jun. 2017, pp. 2723–2727, doi: 10.1109/PVSC.2017.8366708.

[14] H. Cha, B. Bhang, S. Park, J. Choi, and H. Ahn, "Power prediction of bifacial Si PV module with different reflection conditions on rooftop," *Appl. Sci.*, vol. 8, no. 10, p. 1752, Sep. 2018.

[15] P. Babal, M. Korevaar, S. Franken, J. Mes, T. Bergmans, and K. Wilson, "Uncertainties in irradiance measurements of sensors to POArear of bifacial solar panels," in *Proc. 47th IEEE Photovoltaic Spec. Conf. (PVSC)*, Jun. 2020, pp. 0959–0963, doi: 10.1109/PVSC45281.2020.9301008.

[16] S. Roest, W. Nawara, B. B. Van Aken, and E. G. Goma, "Towards developing a standard for testing bifacial PV modules: Single-side versus double-side illumination method I-V measurements under different irradiance and temperature," in *Proc. IEEE 44th Photovoltaic Spec. Conf. (PVSC)*, Jun. 2017, pp. 3462–3467, doi: 10.1109/PVSC.2017.8366734.

[17] J. Lopez-Garcia, E. Ozkalay, R. P. Kenny, L. Pinero-Prieto, D. Shaw, D. Pavanello, and T. Sample, "Implementation of the IEC TS 60904–1–2 measurement methods for bifacial silicon PV devices," *IEEE J. Photovolt.*, vol. 12, no. 3, pp. 787–797, May 2022.

[18] J. F. Martínez, M. Steiner, M. Wiesenfarth, G. Siefer, S. W. Glunz, and F. Dimroth, "Power rating procedure of hybrid concentrator/flat-plate photovoltaic bifacial modules," *Prog. Photovolt., Res. Appl.*, vol. 29, no. 6, pp. 614–629, Jun. 2021.

[19] B. G. Bhang, W. Lee, G. G. Kim, J. H. Choi, S. Y. Park, and H.-K. Ahn, "Power performance of bifacial C-Si PV modules with different shading ratios," *IEEE J. Photovolt.*, vol. 9, no. 5, pp. 1413–1420, Sep. 2019.

[20] B. Meng, R. C. G. Loonen, and J. L. M. Hensen, "Data-driven inference of unknown tilt and azimuth of distributed PV systems," *Sol. Energy*, vol. 211, pp. 418–432, Nov. 2020.

[21] B. Yang, H. Ye, J. Wang, J. Li, S. Wu, Y. Li, H. Shu, Y. Ren, and H. Ye, "PV arrays reconfiguration for partial shading mitigation: Recent advances, challenges and perspectives," *Energy Convers. Manag.*, vol. 247, Nov. 2021, Art. no. 114738.

[22] I. Sarbu and C. Sebarchievici, *Solar Heating and Cooling Systems: Fundamentals, Experiments and Applications*. Cambridge, MA, USA: Academic Press, 2016.

[23] I. Dincer, *Comprehensive Energy Systems*. Amsterdam, The Netherlands: Elsevier, 2018.

[24] U. Yusufoglu and A. Halm, "Modeling and simulation of annual energy yields of bifacial modules at different climate zones," in *Proc. 2nd Bifacial PV Workshop*, 2014.

[25] M.-S. Won, C. P. Langcuyan, and Y.-C. Gao, "A study on the utilization of clayey soil as embankment material through model bearing capacity tests," *Appl. Sci.*, vol. 10, no. 7, p. 2315, Mar. 2020.

BYEONG GWAN BHANG received the B.S. and M.S. degrees in electrical engineering from Konkuk University, Seoul, South Korea, in 2017 and 2019, respectively, where he is currently pursuing the Ph.D. degree with the Next Generation Photovoltaic Module and Power System Research Center. His research interests include utility of FPVs, MPVs, and their operations and maintenance using big data analysis.

JIN HEE HYUN received the B.S. and M.S. degrees in electrical and electronic engineering from Konkuk University, Seoul, South Korea, in 2019, where she is currently pursuing the Ph.D. degree with the Next Generation Photovoltaic Module and Power System Research Center. Her research interest includes high power density PV module, such as shingled module and its application in floating and marine PVs.

SEONG-HYEON AHN is currently pursuing the B.S. and M.S. degrees in electrical engineering with the Next Generation Photovoltaic Module and Power System Research Center, Konkuk University, Seoul, South Korea. His research interests include PV power system diagnosis with power index and fusion of renewable energy resources with an emphasis on floating and marine photovoltaics.

JIN HO CHOI received the B.S. and M.S. degrees in electrical engineering, in 2018 and 2019, respectively. He is currently pursuing the Ph.D. degree with the Next Generation Photovoltaic Module and Power System Research Center, Konkuk University, Seoul, South Korea. His research interests include power prediction and fault detection of floating and marine photovoltaics using high-density PV module (HDM).

GYU-GWANG KIM received the B.S. and M.S. degrees in electrical engineering from Konkuk University, Seoul, South Korea, in 2016 and 2019, respectively, where he is currently pursuing the Ph.D. degree in electrical engineering. He is also working with Chungbuk Techno Park (CBTP), Chungbuk, South Korea. His current research interests include PV output model and O&M applied to various environmental conditions, including ground, floating, and marine.

HYUNG-KEUN AHN (Member, IEEE) received the B.S. and M.S. degrees in MOSFETs in electrical engineering from Yonsei University, Seoul, South Korea, in 1983 and 1985, respectively, and the Ph.D. degree in HEMTs from the Department of Electrical Engineering, University of Pittsburgh, Pittsburgh, PA, USA, in 1993. From 1986 to 1995, he was with LG Semiconductor Company, working on silicon-based device design and process integration. In 1995, he joined the Department of Electrical Engineering, Konkuk University, Seoul. He was the first National Photovoltaic Research and Development Program Director of the Ministry of Knowledge Economy, South Korea, from 2009 to 2011. From 2014 to 2016, he was also a Foreign Professor at the Department of Electrical and Control Engineering, Division of EE, Shandong University of Technology (SDUT), Zibo, Shandong, China. He is currently a Professor and the Dean of the Next Generation PV Module and Power System Research and Development Center. He is also working on design of microgrid network for net-zero energy house and town using EMS, ESS, bifacial and shingled PV modules, and applicable to floating and marine PVs under the demand response control. His research interests include reliability of both Si and GaAs-based solar cells and PV modules for applications in micro roof-top to large scale of PVs connected with ESS, focusing on failure analysis, reliability, and maintenance, repair, and operation (MRO). He has been a Committee Member of the National Science and Technology Commission, Energy Department, since 2005.